ARMY RESEARCH LABORATORY

Investigations on the Broadband Shielding Effectiveness of Metallized Glass Fiber

by William O. Coburn, John Latess, Christian G. Reiff, Vincent J. Ellis, James Stewart, and Calvin D. Le

ARL-TR-1376   March 1998

19980324 089

Approved for public release; distribution unlimited.

DTIC QUALITY INSPECTED 4

Army Research Laboratory

Adelphi, MD 20783-1197

Investigations on the Broadband Shielding Effectiveness of Metallized Glass Fiber

William O. Coburn, John Latess, Christian G. Reiff, Vincent J. Ellis, James Stewart, and Calvin D. Le
Sensors and Electron Devices Directorate

Abstract

Metallized glass fiber (MGF) is a glass fiber substrate with a metal coating that can be used to improve the electrical properties of reinforced composites. The material considered here (RoMHOglas™-metallized glass conductive fibers produced by Lundy Technical Center, Pompano Beach, Florida) is an E-glass fiber metallized with Al and processed into a non-woven mat. When formed into a mat, the MGFs lead to an effective sample conductivity, σ_{eff}, which is the parameter of interest for electromagnetic shielding in the RF region. Experimental results are presented that show that σ_{eff} is dependent on the resin and curing process used to produce the MGF samples. The sample conductivity was optimized using polyester resin and vacuum bagging techniques. The lessons learned were used to construct an MGF-shielded Army tactical shelter-size enclosure having no apertures or penetrations other than the door opening.

We applied two layers of the MGF mat to the interior surfaces of a plywood, full-scale model of an Army tactical shelter. Using overlapping seams, we secured the MGF layers to the plywood walls and sprayed them with polyester resin. A vacuum bag was fitted to the interior and exterior of the shelter model. A vacuum was applied to compress the two layers of MGF mat and remove excess resin. A metal door with an eight-cleat clamping arrangement and an electromagnetic interference gasket was used to provide a continuously shielded enclosure. This shielded enclosure was then tested according to IEEE-STD-299-1991, with some modifications, at frequencies up to 17 GHz. The results are presented as recommended by the test standard and indicate that compressed MGF mat can provide roughly 60 dB of attenuation to a distant source, but very little shielding below 10 MHz.

Foreword

This report represents progress in ongoing research to evaluate the effectiveness of metallized glass fiber (MGF) as an electromagnetic shielding solution. We are primarily concerned with frequencies below 1 GHz, where the conductivity dominates the response of shielding materials. For this reason, our initial efforts were concentrated on near-field measurements to determine the conductivity of MGF samples as a function of the curing process. Wideband pulse attenuation is also discussed as a useful technique to estimate plane wave shielding. The lessons learned are used to construct an MGF-shielded, full-scale model of an Army tactical shelter. This MGF enclosure is tested in a manner consistent with IEEE-STD-299-1991, at frequencies up to 17 GHz. The results of these different investigations are compiled here to provide a comprehensive review of our efforts in evaluating the shielding effectiveness of MGF materials.

Contents

Preceding Page Blank

Figures

Tables

1. Introduction

Metallized glass fiber (MGF) is a glass fiber substrate with a metal coating that is manufactured as a multifilament continuous strand. MGF can be processed into typical fiberglass reinforcement configurations and used to modify the properties of polymeric composites [1]. MGF can be incorporated to improve the thermal and electrical conductivity of reinforced composites, and an optimum design can retain the desired physical properties [1,2]. The U.S. Army Research Laboratory (ARL) is interested in evaluating such materials as an alternative to metals for electromagnetic (EM) shielding [3]. MGF in a random orientation mat could provide good electrical properties that are roughly isotropic at frequencies below a few hundred megahertz.

The material considered here (the product name is RoMHOglas™) is an E-glass fiber (average diameter 0.7 mil) metallized with aluminum (Al). RoMHOglas™ is available from Lundy Technical Center, Pompano Beach, Florida, in 36-in.-wide rolls of nonwoven mat ($\frac{1}{2}$ or $\frac{1}{4}$ oz/ft^2). The thickness of the mat is nonuniform but is estimated to be $\frac{1}{16}$ in. in its relatively compressed state when taken off the roll. The metallized layer is a continuous Al film bonded to the glass fiber with 50 to 100 percent coverage. The average dc resistance of the monofilament MGF is 2.5 Ω/cm; and by weight, the mat is 37 percent glass and 63 percent Al [1].

Assuming a uniform Al coating on an 18-μm-diameter fiber substrate and a conductivity, $\sigma_{Al} = 2.9 \times 10^7$ S/m. The above dc resistance implies a metal thickness, $d \approx 0.25$ μm. The EM absorption in the Al layer depends on the skin depth, $\delta_{Al} = 1/\sqrt{\pi\mu\sigma_{Al}f}$, where μ is the permeability and f is frequency. The absorption in one Al layer is small (compared to the surface reflection) because δ_{Al} is much greater than d for the frequencies of interest. When formed into a mat, the MGF leads to an effective sample conductivity, σ_{eff} (which is the parameter of interest for EM reflection) and relative permittivity, ε_r. For cured samples, this σ_{eff} increases exponentially with the MGF loading density, and we determine σ_{eff} from the measured shielding effectiveness (SE), under conditions for which the exact solution is available. Previous results for the EM characterization of RoMHOglas™ indicate that for cured samples of MGF mat (i.e., high loading densities), $\sigma_{eff} \approx 1000$ to 2000 S/m [4]. However, this is dependent on the curing process, and uncured samples exhibit practically no EM reflection at these frequencies because they have an extremely low σ_{eff}. In general, σ_{eff} will dominate the material's EM response for frequencies where $f << \sigma_{eff}/(2\pi\varepsilon_0\varepsilon_r)$; even for uncured samples, the influence of ε_r on the EM response is negligible below microwave frequencies.

The remainder of this report is organized as follows: First, we summarize experimental techniques and corresponding theory, with references provided for the interested reader. Second, we describe the analysis techniques used for comparison to the measured data, where a knowl-

edge of σ_{eff} is assumed to be adequate for determining a material's EM response. Third, we present the test results and some comparisons to theory for magnetic (H) field, plane wave, and enclosure SE. Finally, we present a summary and conclusions for the broadband shielding applications of MGF.

2. Experimental Methods

The nonconductive and/or anisotropic features of advanced composite materials complicate the characterization of material EM properties and system response modeling. Common techniques, which use shielded rooms, coaxial holders, or other types of measurement fixtures, typically rely on a low-contact impedance between the sample material and test fixture. Typical composites do not provide a means to make good electrical contact between the conducting members (inherent and/or introduced) of the composite material and test fixtures. This raises questions regarding the applicability or reliability of traditional test methods for composite samples. For this reason, we have focused on measurement techniques that do not require conductive contact in order to obtain information on the EM properties of the material under test. The experimental methods include near-field insertion loss, wideband pulse attenuation, and standard SE test methods.

We concentrated our initial efforts on developing techniques to accurately measure the σ_{eff} of various composite samples. Once determined, the material's EM response can be analytically predicted and the relative shielding performance of the samples evaluated. Near-field insertion loss measurements were conducted on MGF samples, which were cured in different ways, at frequencies below 1 GHz, where conductivity dominates the response of shielding materials. The samples included uncured MGF mat under vacuum (0, 5, or 28 in. Hg) and cured MGF mat using polyester or epoxy resin under different vacuum conditions (0, 5, or 28 in. Hg). The wideband pulse attenuation method provides insertion loss information in the frequency range 500 to 6000 MHz. Attenuation measurements were conducted on an uncured MGF mat and on an MGF mat cured using polyester resin and high vacuum (28 in. Hg). The enclosure SE test method is based on IEEE-STD-299-1991, which covers the frequency range 14 kHz to 18 GHz. The enclosure interior was shielded with two layers of MGF mat cured using polyester resin and low vacuum (5 in. Hg).

2.1 Near-Field Technique

In an effort to measure σ_{eff} of small planar composite samples, we investigated the utility of the magnetic near-field or eddy current measurement technique. The near-field measurement technique is capable of providing data from which conductivity information can be extracted. This technique does not require electrical contact with the sample under test and is therefore ideal for characterizing composite materials.

2

2.1.1 Theory

The first step taken in understanding how an eddy current measurement might be used to evaluate the conductivity of composite samples was to examine the fields produced in the near field of electrically small loop antennas. These fields are given by [5]

$$B_\theta = \frac{-\mu_o \beta^2 m}{4\pi r}\left(1 - \frac{j}{\beta r} - \frac{1}{\beta^2 r^2}\right)e^{-j\beta r}\sin\theta \ ,$$

$$B_r = \mu_o \beta^2 \frac{m}{2\pi r}\left(\frac{j}{\beta r} + \frac{1}{\beta^2 r^2}\right)e^{-j\beta r}\cos\theta \ ,$$

$$\tag{1}$$

$$E_\phi = 377\beta^2 \frac{m}{4\pi r}\left(1 - \frac{j}{\beta r}\right)e^{-j\beta r}\sin\theta \ ,$$

where the plane of the loop is centered and normal to the polar axis of the spherical coordinate system. The fields have azimuthal symmetry with the field point located by spherical coordinates (r,θ), and $m = I_o NA$ is the magnetic moment, where

N is the number of turns,
$A = \pi a_1^2$ is the area of the loop,
I_o is the current on the loop,
$\beta = 2\pi/\lambda$ is the propagation constant in free space,
r is the distance from the loop center to the observation point, and
θ is the polar angle measured from the vertical.

These equations illustrate the potentially useful characteristics of a near-field measurement. If the distance r from the antenna is kept below $\lambda/2\pi$, the magnetic field falls as $1/r^3$. The fields in the region $r < \lambda/2\pi$ are termed quasi-stationary and do not behave in the same manner as radiated fields. These rapidly decaying fields provide measurement isolation from leakage fields, while using a relatively small test sample and no Faraday enclosure. Using the test configuration shown in figure 1, with a 30-cm^2 sample and the transmitting and receiving antenna centers separated by 2 cm, the leakage path, bb', is nearly 15 times the direct penetration path, a. The fields reaching the receiving antenna due to this leakage path will have attenuated 70 dB while traversing this distance. If the net fields reaching the receiving antenna through the material are larger than the leakage fields, the measurement will indicate the transmitted field level. A measurement of 70 dB isolation is a conservative value, for any fields completing path bb' are partially scattered and not directly radiated.

This effect, while a virtue, also creates practical frequency limitations. As stated above, isolation is obtained from the rapidly decaying fields in the near field of a small loop antenna. The calculated isolation assumes that the fields are falling proportional to $1/r^3$ over the entire 30-cm leakage path distance. This will occur as long as $\lambda/2\pi > 30$ cm. Once $\lambda/2\pi = 30$ cm,

the fields will begin to fall as $1/r$. The frequency at which this occurs is 160 MHz. This technique will work beyond 160 MHz; however, the measurement isolation beyond this frequency will be reduced. Here we consider only nonmagnetic materials, and the reader is referred to Latess et al [4] for the detailed applications and limitations of this technique.

2.1.2   Test Description

In the near-field test setup (fig. 1), we used a Hewlett Packard (HP) 3577A network analyzer as the source and the receiver. The receiving antenna consists of a single-turn, open-circuited loop (r_1 = 2.2 cm). The antenna's open-circuit voltage is measured using a Tektronix P6047 voltage probe. The high-impedance voltage probe prevents current from being formed in the receiving antenna that may affect the measurement. The voltage probe also alleviated impedance-matching problems in the receiving circuit. The transmitting antenna consists of a short-circuited, single-turn loop (r_1 = 2.2 cm) that is driven by the network analyzer via a Tektronix CT-2 current transformer. The transformer is essential to provide high-frequency performance. It performs the impedance matching necessary to reduce resonance effects in the transmitting circuit. These effects lead to radiated fields that are easily picked up by the high-impedance receiving section. The high-frequency performance is necessary to provide enough measurement sensitivity to measure the relatively low conductivity typical of composite samples. The frequency coverage to date extends from 1 kHz to 150 MHz. Low-frequency performance is necessary for highly conductive materials, while the high-frequency performance is required for thin materials with low conductivity values [4].

A reference measurement is taken with the antennas coaxially positioned in free space. A 30-cm^2 test sample is then placed between the two materials, and the open-circuit voltage is measured once again. Swept frequency measurements are performed from 1 kHz to 150 MHz. The difference between the reference and test measurements is computed within the network analyzer and is termed magnetic near-field insertion loss, expressed in decibels. The reference measurement is shown in figure 2. The 20-dB/decade rolloff in the frequency region between 1 and 100 kHz is due to the limited bandwidth of the Tektronix current transformer. Beyond 100 kHz, the reference measurement is reasonably flat, as it should be until 100 MHz. The rising amplitude at 100 MHz is attributed to sources other than the transmitting antenna. Further investigation verified that this effect is noise coupled to the received signal cable and can be eliminated by using optical isolation.

2.1.3   Test Validation

To validate the near-field technique, the results of plane wave SE measurements in a transverse electromagnetic (TEM) cell were compared with plane wave SE analytical solutions using conductivity values determined by the near-field technique. Previous test results [6] have shown that when the laminates are electrically very thin and the fiber separation is a

Figure 1. Magnetic near-field insertion illustration:
(a) experimental configuration,
(b) direct path, and
(c) leakage path.

(a)

Test sample

Transmitting antenna

2 cm

Receiving antenna

30 cm

(b) Direct path

(c) Leakage path

(a) Magnitude (dBm)

Frequency (Hz)

(b) Dynamic range (dB)

Frequency (Hz)
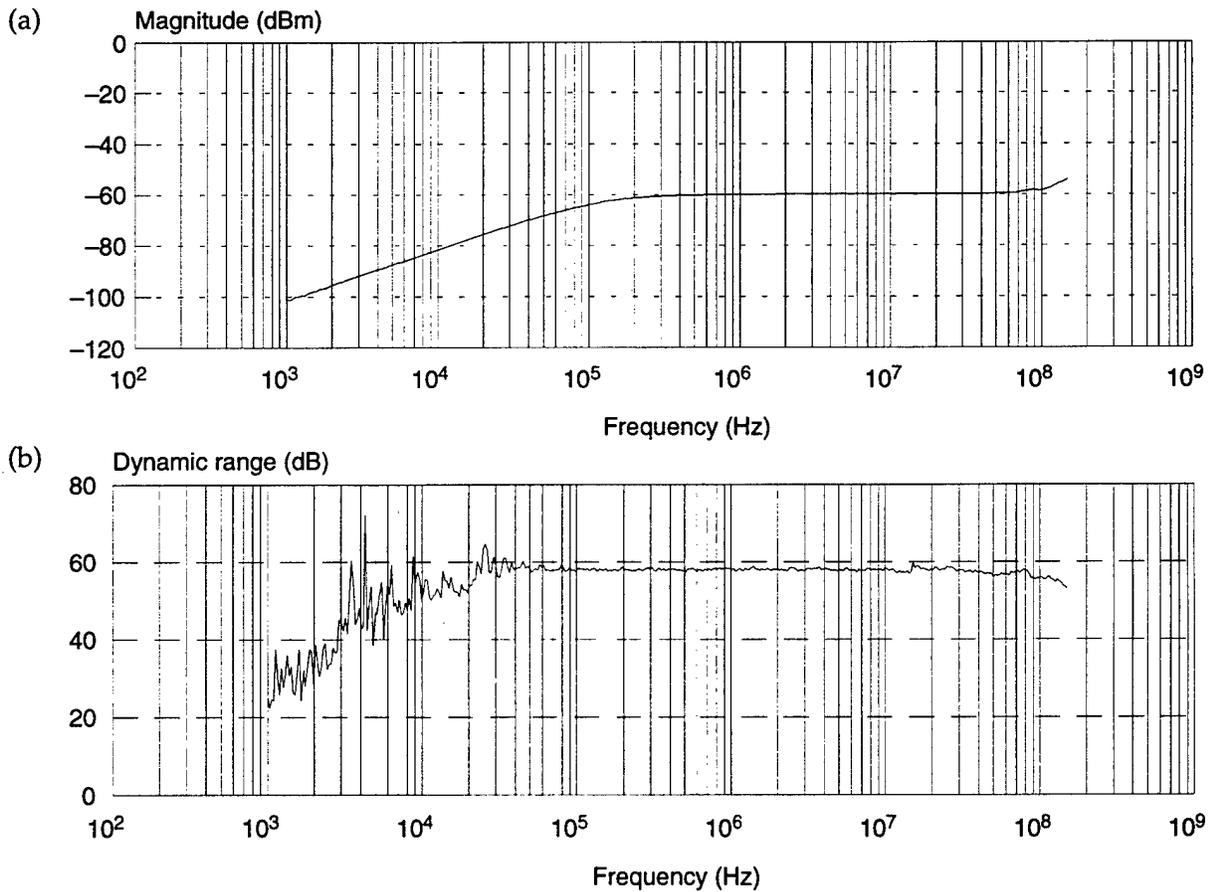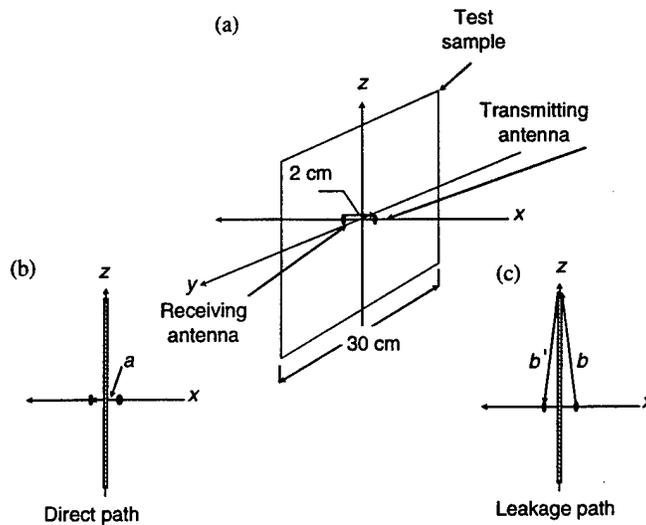
Figure 2. Dynamic range for near-field measurements: (a) reference measurement is for coaxial antennas separated by 2 cm, and (b) dynamic range is difference between reference measurement and measurement for antennas separated by 30 cm.

5

tiny fraction of a wavelength, conductive laminate composites can be modeled as homogenous, isotropic, conducting materials. Then for a given σ_{eff} and cylindrical geometries, H-field SE can be calculated based on the theory of EM field coupling into infinite isotropic cylinders [7]. The H-field SE of finite-length cylinders approaches that of infinitely long cylinders when the length is on the order of the diameter and the H-field is axial (i.e., oriented along the cylinder axis). For finite-length cylinders, the measured H-field SE in the TEM cell produced results within 3 dB of the analytical solution, which is considered good agreement [4]. The close agreement of these results is very encouraging and indicates that the near-field technique can be a valuable tool for measuring σ_{eff} of composite materials. With this knowledge we are able to analytically determine the material's response to various EM environments at low frequencies for which the σ_{eff} concept is appropriate.

2.2   Wideband Pulse Attenuation Measurements

The ARL Scale Model Facility (SMF) was also used to investigate the SE of MGF mat by measuring the "fast" (i.e., wideband) pulse attenuation of a planar sample. The ARL SMF can radiate a repetitive, horizontally polarized E-field pulse with a nominal risetime ≈ 0.2 ns and a pulsewidth $\approx$ 1 ns. Time-domain sampling techniques allow signal averaging of sensor responses, which greatly enhances the signal-to-noise ratio (SNR) of the measured transients. More detailed descriptions of the SMF pulser, EM sensors, calibration techniques, and data compensation algorithms for accurate recording of picosecond regime events are provided by Loftus [8,9]. The test setup is shown in figure 3, which indicates the physical relationship between the source dipole antenna, the MGF barrier, and the field sensor. The sensor responds to the time derivative of the E-field (E-dot), which is shown in figure 4(a) without the MGF barrier in place. The integrated signal is shown in figure 4(b) and this pulse represents the incident plane wave E-field, which is approximately a plane wave.

Our experimental objective was to measure the horizontally polarized E-field pulse with and without the MGF barrier in place between the source dipole and the EM field sensor. The sample is sufficiently large that the pulse attenuation can be measured before observing spurious reflections or edge diffractions. For the MGF barrier, the SE of the sample can be characterized in the frequency range 100 to 2000 MHz [10]. The measured SE for the dry MGF mat provides a reference for the EM properties of this commercially available composite material. We then incorporated an identical MGF mat into a polyester resin matrix, which was cured at ambient temperature under vacuum. This cured sample was then tested in the same manner as the uncured sample. Although the pulse attenuation measurement technique is not directly relatable to standard SE test methods, it provides information on the relative shielding capability of cured and uncured samples.

Figure 3. Physical relationship between dipole, MGF sheet, and sensor: (a) side view and (b) top view.

(a)

MGF sheet

1.5 m   0.3 m

Antenna

Sensor and cable

2.7 m

3.7 m

To sand   To shield room

(b)   1.8 m

MGF sheet

2.7 m

Sensor

Antenna
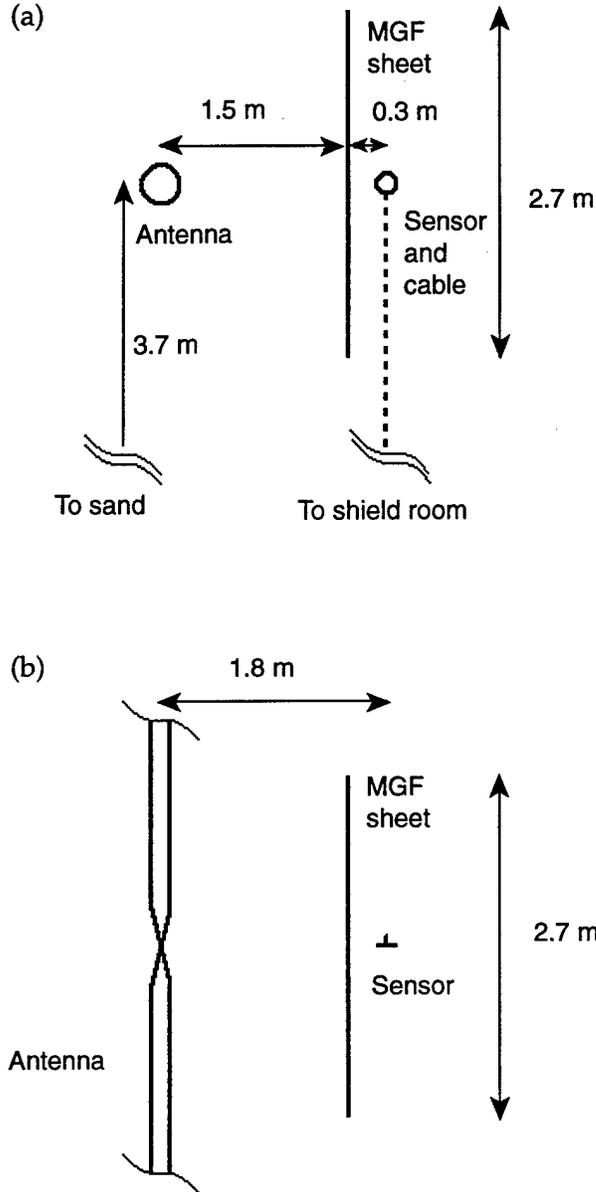
2.2.1 Uncured MGF Mat

A planar sample was constructed from three strips (36 in. wide) of $\frac{1}{4}$ oz/ft^2 RoMHOglas™, taped together with nonconductive tape. The finished mat consisted of three pieces of MGF material that measured 9 × 3 ft, joined on the longest dimension with 3-in. overlapped joints (see fig. 5). Electrical contact between the sheets of nonwoven MGF mat was maintained only by the pressure of the tape on each side of the sample. This approach was designed to model the layup of MGF mat, where no special provisions are made for overlapping laminates. This uncured MGF sample is placed between the source dipole and EM field sensor, which are 3.7 m above the ground (see fig. 3). Polarization effects were not investigated and the results correspond to an incident E-field oriented across the strips of MGF (i.e., across the vertical seams). This corresponds

(a)

4×10^{11}

2×10^{11}

E-dot (V/m/s)

0

-2×10^{11}

Incident E-dot

0   1   2   3   4

Time (ns)

(b)

120
100
80
60
40
20
0
-20

E-field (V/m)

Incident field

0   1   2   3   4

Time (ns)
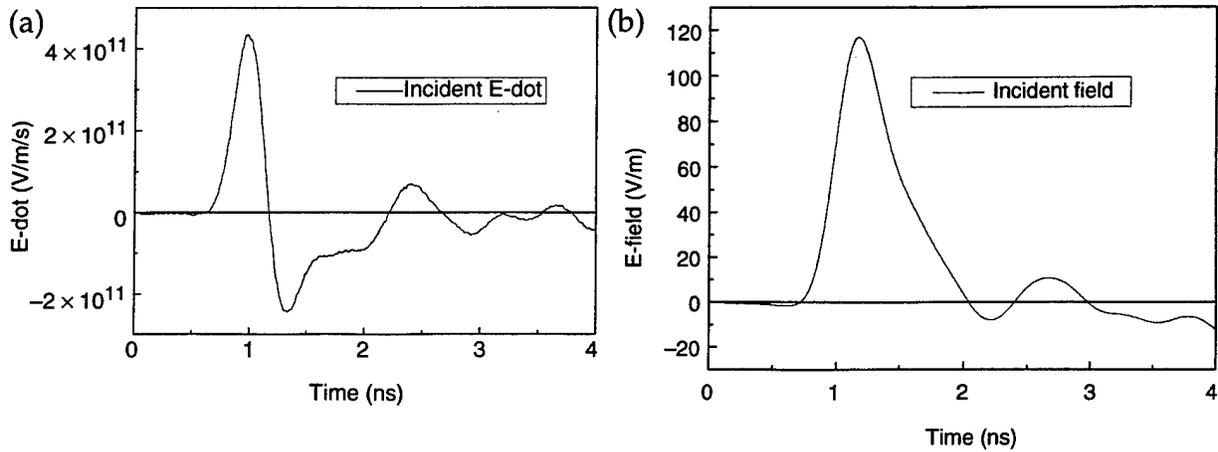
Figure 4. Incident electric field for pulse attenuation measurements: (a) derivative of incident electric field (E-dot) and (b) incident electric field.

Figure 5. MGF mat constructed for wideband pulse attenuation measurements showing seam locations.

9 ft

8 ft, 6 in.
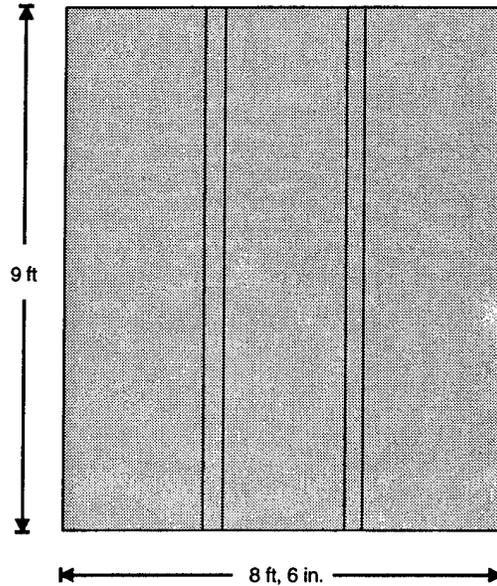
to the worst-case polarization for EM field leakage through the long seams (which are resonant for frequencies above 50 MHz). For uncured samples, the nature of the mat implies a nonuniform and very low surface resistance, owing to the poor electrical contact between the sheets of the MGF.

2.2.2   Cured MGF Mat

We constructed and tested a cured MGF mat to obtain additional information on the processing effects on the EM performance of MGF fibers. The composite mat was cured using a polyester matrix material while under a vacuum of 28 in. Hg. Figure 6 illustrates the configuration used to compress and cure the mat. The measurement sensitivity was optimized by

including a 23-dB preamplifier before the oscilloscope. This amplification aids in overcoming the sampling head noise floor but does not help with the data lost through cable attenuation. The preamplifier, cables, and instrumentation were unchanged, except for in-line attenuators when we measured the fields with and without the MGF mat in place. This ensured that the amplifier characteristics and cable losses cancel when we calculated the SE. Precision attenuators with flat response in the required frequency range were used when measuring the direct field. A factor of 20.3 was used to remove the effects of the attenuators from the data. The SE was calculated from the E-dot data. The timing relation between the measured amplitudes also allowed us to determine the shield diffusion time.

2.3   Shielded Enclosure Full-Scale Model

We constructed a full-scale MGF shelter model for testing and evaluation. The enclosure we chose for this series of tests was a mockup of the hardened standard shelter (HSS). The HSS can be manufactured of fiber-reinforced plastics; it provides protection against blast overpressure, fragmentation rounds, chemical/biological attack, and EM environment effects (E^3). One design for the composite HSS provides EM shielding by an aluminum liner that is welded together and used as a form for filament-wound graphite epoxy (G/E). This aluminum liner is expensive to install and adds weight to the HSS. The potential weight savings of the MGF, in addition to its compatibility with the composite manufacturing process already used with the G/E materials, make this shelter an interesting candidate for evaluating the SE of MGF in this application.

As discussed earlier in the previous two sections of this report, compression of the MGF is required to achieve maximum effective conductivity. These compressive forces are inherent with most, if not all, composite manufacturing processes and contribute directly to the resulting strength of the composite structure. We made an effort to provide the necessary compressive forces to the full-scale shelter mockup to realistically emulate the MGF performance in a real composite structure. This task proved quite difficult, however, since we used only the resources and facilities at hand.

Figure 6. Vacuum configuration used to compress and cure MGF mat.

To vacuum pump

Plastic bagging material

Vacuum valve

Overlapping MGF layers

Vacuum bag sealant tape
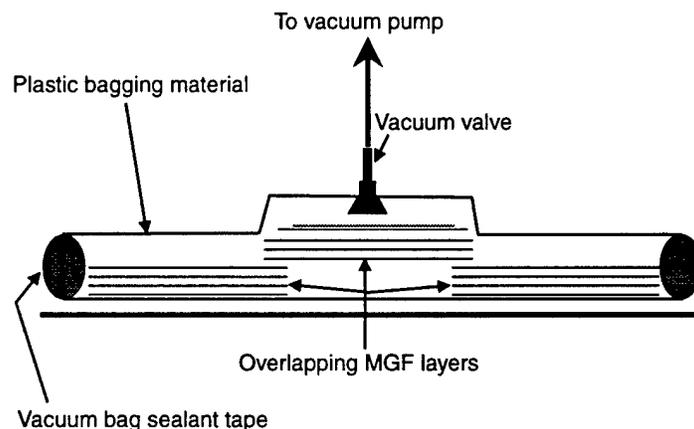
To obtain the required compressive forces, we used a vacuum to compress the MGF to a plywood shelter mockup. Figure 7 illustrates the construction of the plywood "form," which consists of an external 2- × 2-in. wooden frame lined with ¼-in. plywood. The result of this construction was a smooth interior plywood surface on which to place the MGF. The plywood was glued to the frame and held in place with a small number of metal screws.

The vacuum was applied to the MGF via an airtight seal between a shelter inner bag and a shelter outer bag, as illustrated in figure 8. The inner bag was fitted and assembled before the installation of the MGF and polyester resin. Standard vacuum debulking material was used for the inner and outer bags. All seams were sealed using tacky tape, an industry standard. The MGF material was held in place with small staples, and a paint roller proved to be the best approach for applying the polyester resin. The inner bag was then installed and sealed to the outer bag at the door.

Figure 9 illustrates the bag placement. Once the inner bag was positioned inside the shelter, the two bags were joined around the door, and a vacuum was applied to evacuate the area between the two bags. A good vacuum (29 in. Hg) would provide nearly 14.5 psi compressive force on the MGF. Prior laboratory experiments indicated that only 5 in. Hg were

Figure 7. Wooden mold used to construct MGF shelter.
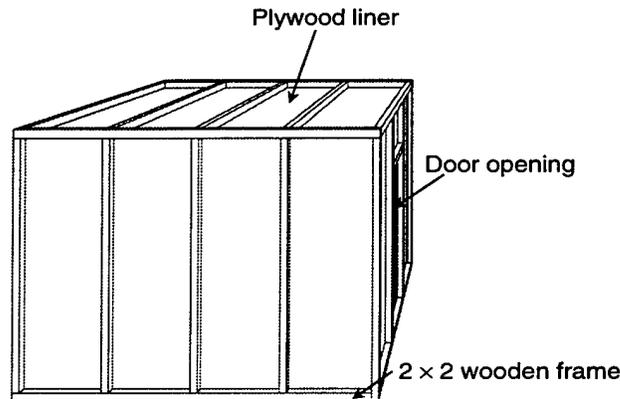
Figure 8. Vacuum bag arrangement.
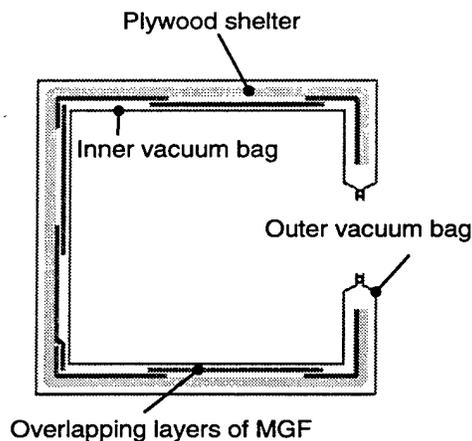
Figure 9.
Configuration of
vacuum bags for
MGF shelter.

Outer vacuum bag

Wooden shelter form   Inner vacuum bag
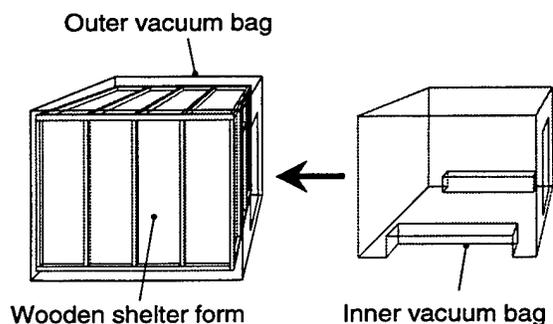
required to obtain near maximum effective conductivity values for the dry MGF material. Because we introduced the resin matrix material with its associated viscosity, we could not achieve maximum effective conductivity values. Polyester resin was an improvement over the epoxy resin; unfortunately, due to the environmental conditions present at the construction site, contamination of the taped bag joints was unavoidable. The resulting vacuum leaks limited the maximum obtainable vacuum to 5 in. Hg or 2.45 psi, which is significantly less than the desired 14.5 psi. One would expect the resulting performance of the shelter to be a lower limit; improved performance could be expected with better manufacturing conditions.

2.3.1   *Low-Range Loop Measurements*

The test approach is to follow IEEE-STD-299-1991, using equipment that had been appropriately calibrated within the past year. IEEE-STD-299-1991 calls for SE tests at seven frequencies in three ranges (high, mid, and low), along with a preliminary spatial scan to disclose serious defects. The measurements were in accordance with IEEE-STD-299-1991, except where indicated. At all frequencies, the substitution technique was used to quantify the measured SE. The preliminary scanning measurements recommended in IEEE-STD-299-1991 were conducted at 20 MHz, which is much less than F_r, and at 300 MHz, which is much greater than F_r. The results indicated no significant problem areas, except the door. Test points near the door showed SE reductions of several decibels, which depended on the pressure applied to the door's contact points. Since the HSS mockup had no other penetrations, the preliminary measurements indicated that all seams had been adequately sealed.

The configuration for the low-range, free-field calibration consisted of coplanar loops with the edges 24.5 in. apart in the absence of the shield. The free-field calibration and test procedures were in accordance with IEEE-STD-299-1991. At each frequency the antenna current was recorded, and the maximum received signal represents the calibration level for this current. The receiver bandwidth was set at the same value used for the SE measurements, which was 1 kHz in all cases. The antenna height was 36 in. above the ground. The low-range test frequencies were selected, based on the available equipment, to be 20 kHz, 200 kHz, 2 MHz, and 10 MHz. The lowest cavity resonant frequency for this enclosure is F_r =

107 MHz, so the chosen frequencies are consistent with IEEE-STD-299-1991 requirements.

The low-range measurement procedure was in accordance with IEEE-STD-299-1991, so the edge-to-edge antenna separation is 24.5 in. In all cases, we used coplanar orientation of the loop antennas. We chose multiple test points to evaluate the SE of each shelter face, the corners, and around the door. However, the number of seams required for the installation of the MGF precluded the use of the test locations specified in IEEE-STD-299-1991. One test point (TP) at the center of each side was chosen as a representative panel measurement, and we scanned the nearby seams using the recommended technique. The low- and mid-range TP locations are indicated in figure 10.

The transmit antenna remained at the required polarization (horizontal (H) or vertical (V), with respect to the ground), while the receive antenna was displaced and rotated. The largest reading (i.e., the minimum SE) was recorded for each TP at each frequency. The TP, antenna polarization, and location are described in table 1. The locations in the corners (C1 and C2) are accessible and were tested as recommended in IEEE-STD-299-1991, with horizontal polarization of the coplanar loop antennas.

2.3.2 *Mid-Range Dipole Measurements*

We used a log-periodic antenna rather than a dipole transmitter for the mid-range, free-field measurements. The distances specified in IEEE-STD-299-1991 were modified somewhat to account for this larger antenna (roughly 2 ft in length). Several different receive antennas were evaluated based on the spatial variations and repeatability of the measured SE. The receive antenna used for the actual testing was a center-fed dipole with a total length of 6 in. Although this antenna is much larger than specified in the test standard at 900 MHz (i.e., 2λ rather than $\lambda/6$), the data appeared to be repeatable and consistent throughout the enclosure. The center of the receive dipole was 1 ft from the outside shelter wall, while the center of the transmit antenna was 5 ft from this wall. The antenna separation (center to center) for calibration was then 4 ft (1.3 m), and the recommended scanning procedure was used. The antenna separations were consistent with IEEE-STD-299-1991, and the recommended calibration procedures were used in addition to a true free-space calibration (i.e., in the absence of the shelter). The variations we observed during these calibration procedures were 1 to 3 dB.

At each frequency the transmit antenna current was recorded. The average of the maximum and minimum received signal is the calibration level for this input current. The receiver bandwidth was set at the same value used for the SE measurements, which was 1 kHz in all cases. The antenna height was 36 in. above the ground. The selected test frequencies were 600 and 900 MHz, which are greater than $3F_r$, in addition to 300 MHz, which is $\cong 3F_r$. During the SE measurements, the receive antenna center was kept 1 ft from the inside wall surface, while the transmit antenna center was kept 4 ft from the outside wall surface. The center-to-center

Figure 10. Test point and seam locations.
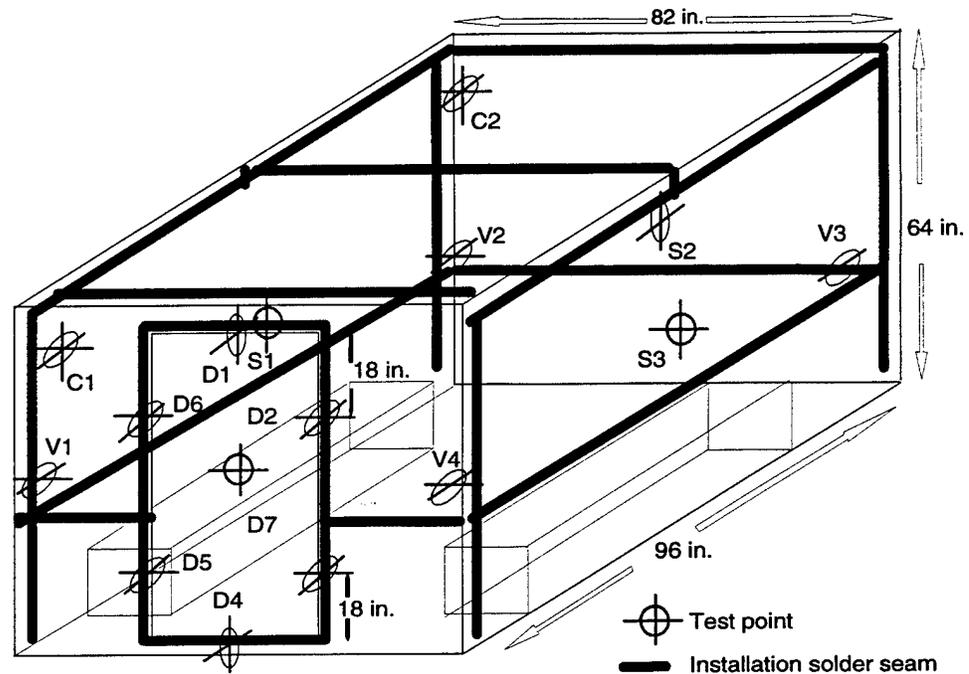
Table 1. Test point locations and antenna polarization for low- and mid-range SE measurements.

TP	Description	Location on HSS (see fig. 10)	Transmitting antenna orientation[a,b]	Receiving antenna orientation[a,b]
C2	Triple corner	Intersection of front, roadside and top planes	H,V	Diagonal
D1	Door top	Top door seam	V	H, V
D2	Right seam, top	Curbside door seam near top	H	H, V
D3	Right seam, bottom	Curbside door seam, bottom	H	H, V
D4	Door bottom	Bottom door seam	V	H, V
D5	Left seam, bottom	Roadside door seam, bottom	H	H, V
D6	Left seam, top	Roadside door seam near top	H	H, V
D7	Door center	Center of door	H, V	H, V
S1	Roadside wall	Center of roadside wall	H, V	H, V
S2	Front wall	Center of front wall	H, V	H, V
S3	Curbside wall	Center of curbside wall	H, V	H, V
V2	Vertical corner	Center of front and roadside plane corner	H, V	H, V

[a]*With respect to ground plane.*
[b]*Perpendicular orientation of receive antnna, also used during scanning procedure.*
Note: H = horizontal; V = vertical

antenna separation was then 5 ft. The wall thickness (0.5 in.) and the difference between calibration and measurement antenna separations are neglected, as recommended in IEEE-STD-299-1991. Variations of the recommended procedures were investigated, such as calibrations in free-space versus near the shelter, and variations in the antennas and antenna separations used. These experiments resulted in a 1- to 3-dB difference in

13

received signal between the calibration and measurement configurations. This small difference is also typical of the variations observed during the calibration and measurement scanning procedures. The use of an average of the calibration measurements and recording the maximum received signal for the SE measurements, as recommended in IEEE-STD-299-1991, minimizes the importance of these small variations.

The mid-range measurement procedure is consistent with IEEE-STD-299-1991, except for the LP transmit antenna. Each TP was tested using both polarizations of the transmit and receive antennas and the recommended scanning technique. In the scanning procedure, the transmit antenna remained at a fixed polarization while the receive dipole was displaced and rotated. The largest reading was recorded for each TP at each frequency and polarization. The recorded measurement data (i.e., the minimum SE) were typically 2 to 3 dB less than the best measurement (i.e., the highest SE) and were observed near the seam locations.

2.3.3   High-Range Horn Measurements

The MGF enclosure was tested at high frequencies (>1 GHz) following the procedures specified in IEEE-STD-299-1991, with few exceptions. Although the standard calls for a 200-W amplifier, we used 20-W amplifiers. We did not use an isolator on the source, and we used a spectrum analyzer as the detector, in place of a field strength meter. The test frequencies were 1, 9, and 17 GHz. All measurements were made in the center of the interior of the shelter, with the receiving horn pointing in the direction of the source. In all cases, we attempted to orient the source waveguide perpendicular to the gross feature under investigation (i.e., seams, corners, triple-corners, etc). Both horizontal and vertical source polarizations were used and, for every measurement, the minimum received shielding and receive antenna orientation were recorded. The test point locations for the high-range SE measurements are shown in table 2, using the nomenclature of figure 10.

Table 2. Test point locations for high-range SE measurements.

Test point	Description	Location
C1	Triple corner	Intersection of rear, roadside, and top planes
C2	Triple corner	Intersection of front, roadside, and top planes
D1	Door top	Top seam between door and rear plane
D7	Door center	Center of door
D8	Door left	Door roadside, center of vertical door seam
S1	Roadside wall	Center of roadside wall
S2	Front wall	Center of front wall
S3	Curbside wall	Center of curbside wall
T1	Top horizontal corner	Center of top and front plane corner
T2	Top horizontal corner	Center of top and roadside plane corner
V1	Vertical corner	Center of rear and roadside plane corner
V2	Vertical corner	Center of front and roadside plane corner
V3	Vertical corner	Center of front and curbside plane corner
V4	Vertical corner	Center of rear and curbside plane corner

The calibration procedure we used is specified in IEEE-STD-299-1991. The receive horn was placed 3.4 ft (i.e., half the shelter width) in front of the shelter door and the transmit waveguide was placed 6.56 ft in front of the receive horn. Both transmit and receive antennas were placed 3 ft above ground for all calibration and testing. This 3-ft height places the receive antenna at the center (height) of the shelter interior. Calibration was performed for all combinations of source/receive antenna polarizations (vertical-vertical, vertical-horizontal, horizontal-vertical, and horizontal-horizontal). Parallel polarization (pol) configurations were nearly identical (<2 dB variance), and the cross-pol configurations were seen to be approximately 25 dB down from the parallel-pol configurations. Additionally, the calibrations were performed with and without the metal door on the shelter, directly behind the receive antenna. The effect of the door on the calibration data was less than 2 dB, with received power being the same or higher with the door present.

3. Analysis

A material's intrinsic properties—conductivity, σ; permeability, μ; and permittivity, ε—determine how the material will interact with EM energy. The effects that the individual intrinsic properties have on a material's shielding performance depend on the characteristics of the EM energy. The relationship between a material's shielding performance and its intrinsic properties, and the characteristics of the EM energy, are provided by EM shielding theory. A widely accepted theory of EM shielding that originated with Shelkunoff [11–13] provides equations relating the intrinsic properties of a material with its shielding performance. This shielding theory was originally developed for the case of plane-wave incident fields. By making certain approximations, we can modify the theory to apply to the general case of EM fields emanating from magnetic (low-impedance) sources, as well as electric (high-impedance) sources. The results of this theory are summarized below.

The total attenuation, L_{total} (in dB), of an EM wave due to a shielding barrier is defined as the sum of the reflection loss, R (in dB), absorption loss, A (in dB), and re-reflection loss, B (in dB):

$$L_{\text{total}} = R_{dB} + A_{dB} + B_{dB} \, . \tag{2}$$

These loss factors are illustrated in figure 11 and depend on the geometry, the intrinsic properties of the material, and the characteristics of the incident EM energy. The total loss is the difference between the incident EM energy and the transmitted EM energy, which is commonly referred to as SE. The reflection loss is a function of the incident wave impedance, Z_w, and the impedance of the shield barrier, Z_s. The reflection loss is defined as

$$R_{\text{dB}} = 20 \log_{10}\left(\frac{(1+K)^2}{4K}\right) , \tag{3}$$

Figure 11. EM shielding theory loss factors.
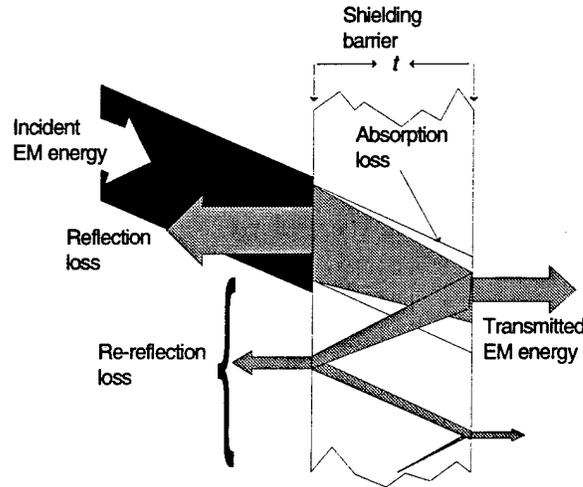
where $K = Z_w/Z_s$. The incident wave impedance is defined as

$$Z_w = \frac{E}{H} = kZ_0 = k\sqrt{\frac{\mu_o}{\varepsilon_o}} = 120\ \pi\Omega\ , \tag{4}$$

where $k = 1$ for a plane wave or a far-field source ($r \geq \lambda/2\pi$), r = distance from source to shield, and λ = wavelength. Otherwise, $k \approx \lambda/2\pi r$ in the near field of a low-impedance source ($r \leq \lambda/2\pi$), and $k \approx 2\pi r/\lambda$ in the near field of a high-impedance source ($r \leq \lambda/2\pi$). Note that Z_w is dependent on the field source, as well as the relative position to that source and the frequency of the source driver.

The shield impedance is defined as

$$Z_s = \frac{\sqrt{\dfrac{j\omega\mu}{\sigma + j\omega\varepsilon}}}{\left(1 - e^{-t/\delta}\right)}\ , \tag{5}$$

where

$\mu = \mu_o\mu_r$ is the permeability (H/m),
$\varepsilon = \varepsilon_o\varepsilon_r$ is the permittivity (F/m),
$\mu_o = 4\pi \times 10^{-7}$ H/m and μ_r is the relative permeability,
$\varepsilon_o = 8.85 \times 10^{-12}$ F/m and ε_r is the relative permittivity,
σ = conductivity (S/m),
t = material thickness (m),
$\delta = (\pi f \mu \sigma)^{-1/2}$ = skin depth (m),
f = frequency (Hz), and
$\omega = 2\pi f$ is the angular frequency (rad/s).

The absorption loss is the amount of energy lost in passing through a shield of thickness t. The field attenuation is due to energy lost from the ohmic generation of exothermic heat. The absorption loss is defined as

$$A_{dB} = 20 \log_{10} |e^{\gamma t}|\ , \tag{6}$$

where $\gamma = \sqrt{(j\omega\mu(\sigma + j\omega\varepsilon))}$ is the propagation constant.

16

The re-reflection loss is the amount of energy lost from multiple reflections of the EM wave inside the shielding barrier. The same reflection and absorption losses (see eq (3) and (6), respectively) are applied to the energy remaining in the material after the initial reflection and absorption loss. All the energy attenuation not included in the initial reflection and absorption loss is included in this factor. This loss factor is defined as

$$B_{dB} = 20 \log_{10} \left| 1 - \frac{(K-1)^2}{(K+1)^2} e^{-2\gamma t} \right| .$$ (7)

These equations provide insight on the importance of each of the intrinsic properties σ, μ, and ε on the overall shielding performance of a material. Making a determination that one is more influential than another is not trivial if the equations are taken for the general case, i.e., any field source at arbitrary frequency and distance from the shielding barrier. The problem is simplified if limited to plane-wave incident fields at frequencies below 1000 MHz. This restriction is justifiable because it includes the EM sources of interest, namely, lightning and nuclear electromagnetic pulse. In the case where the effective media concept is reasonable, this transmission line theory of shielding can be used with the effective material parameters.

3.1 SE Based on Effective Conductivity

Although we claim to measure the effective conductivity directly at low frequencies, it is also useful to estimate this parameter based on the basic material structure. Given the physical structure, the conductivity of constitutive materials, thickness, volume fractions, etc, we can estimate the material's effective electrical parameters. Of course, this approach holds only where the uniformity and isotropic assumptions are valid. For many composite matrix or layered materials, this approach is typically sufficient for engineering results.

3.1.1 *Uncured MGF Mat*

One possible model for the SE of an uncured mat is an extremely low σ_{eff} combined with some EM absorption in the metallized Al layers. Table 3 shows the calculated reflection, R, versus frequency for σ_{eff} = 10 and 100 S/m. The uncompressed nonwoven MGF mat is roughly $\frac{1}{16}$ in. thick and could contain, at most, 90 fibers oriented perpendicular to and stacked across the sample thickness. For uncured samples, the MGF are not in close contact and 45 fibers across the sample thickness might be a better estimate. In the limiting case of 50 percent Al coverage on each fiber, we would have 45 Al layers, whereas for 100 percent coverage we would have 90 Al layers. Included in table 3 is the calculated absorption, A, for an EM wave passing through 45 and 90 Al layers, each with an individual thickness of 0.24 µm. The nonwoven MGF mat actually has a random and twisted fiber orientation, so that A could be highly nonuniform over the sample. We consider an Al thickness of 10.8 µm to charac-

Table 3. Calculated absorption, reflection, and combined SE for uncured MGF.

Frequency (MHz)	A (dB)		R (dB)		SE for 45 layers (dB)	
	45 layers $d = 10.8\ \mu m$	90 layers $d = 21.6\ \mu m$	$\sigma_{eff} = 10$ (S/m)	$\sigma_{eff} = 100$ (S/m)	$\sigma_{eff} = 10$ (S/m)	$\sigma_{eff} = 100$ (S/m)
100	10	20	21	31	31	41
300	18	35	16	26	33	43
500	23	45	14	24	36	46
1000	32	63	11	21	43	53
2000	45	89	8	18	53	63

terize A, and a low σ_{eff} to characterize R. For comparison to the measured SE of uncured MGF, A for 10.8 μm of Al and R for $\sigma_{eff} = 10$ or 100 S/m are combined to form the total SE neglecting multiple reflections (see table 3).

3.1.2 *Cured MGF Mat*

The effective conductivity model for a cured MGF mat would be the same, except the conductivity would be much larger and the thickness would decrease compared to an uncompressed mat. Based on laboratory measurements, we estimate $\sigma_{eff} \approx 1000$–$5000$ S/m, depending on the curing process, with a typical value of 1000 S/m. Because the MGF is compressed, the absorption in the Al layers should also increase since these layers are now in close contact. For a two-layer panel having a total thickness of $\frac{1}{16}$ in. (1.6 mm), table 4 shows the absorption versus the assumed effective conductivity of the MGF sample. For comparison to the measured SE of cured MGF, A (for a thickness of 1.6 mm) and R are calculated for $\sigma_{eff} = 1000$, 2000, and 5000 S/m (see table 4). The total SE neglecting multiple reflections is the sum of these two loss factors (in dB).

3.2   SE Based on Transfer Impedance

Enclosures composed of composite material surfaces were modeled using EMA3D, a three-dimensional (3D) time-domain finite difference (TDFD) Maxwell equation solver, developed by Electro Magnetic Applications, Inc. (EMA) [14]. The composite surface formalism uses a one-way, frequency-dependent transfer impedance function that leads to a series of time-dependent operators [15]. The one-way transfer impedance means that coupling is only accurately modeled from the front to the back of the surface with respect to the impinging energy. For enclosures, this implies that all sources must be either inside or outside the enclosure, but not both. For the continuous enclosures considered here, this limitation is not a concern since the sources are all outside the enclosure. The two-layer MGF shelter is modeled as continuous composite surfaces having $\sigma_{eff} = 2000$ S/m, $\varepsilon_r = 10$, and a total thickness of $\frac{1}{16}$ in. Although $\varepsilon_r = 10$ is not representative of glass fiber, a large value was used to investigate the influence of this parameter on the EM shielding properties. The results of this study indicated that the EM coupling was insensitive to these parameter variations over the range of $\varepsilon_r = 1 - 10$. The incident plane wave E-field is shown in figure 12, where the pulse parameters are chosen to

Table 4. Calculated absorption and reflection for cured MGF mat.

Frequency (MHz)	A (dB)			R (dB)		
	$\sigma_{eff} = 1$ (kS/m)	$\sigma_{eff} = 2$ (kS/m)	$\sigma_{eff} = 5$ (kS/m)	$\sigma_{eff} = 1$ (kS/m)	$\sigma_{eff} = 2$ (kS/m)	$\sigma_{eff} = 5$ (kS/m)
100	8	13	19	37	41	47
300	15	22	33	34	38	43
500	19	28	43	33	36	41
1000	28	40	61	30	33	38
2000	40	55	87	27	31	35

Figure 12. Normally incident electric field for 3D-TDFD simulations of MGF shelter.
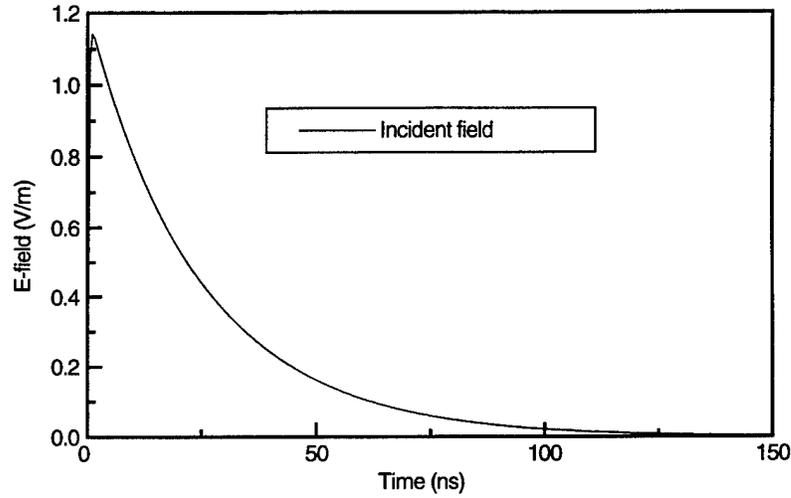
obtain a broadband illumination. The enclosure is in free space, illuminated by a horizontally polarized plane wave pulse incident at a grazing angle (i.e., normally incident on the shelter front face).

4. Results

The results are presented in terms of the magnetic field SE, the plane wave SE, and the enclosure SE for the MGF samples tested. For low-frequency magnetic field shielding, we show that the SE is extremely sensitive to the curing process, which is parameterized by the resulting effective conductivity of the cured sample. For plane-wave shielding at mid- and high frequencies, we show that shielding theory can be used to estimate an MGF material's SE for planar samples. For enclosure shielding we propose that a material's performance is best evaluated by standard test techniques, because the SE is typically dependent on the enclosure construction. The results for a 3D-TDFD simulation of plane wave coupling to an MGF enclosure are shown to demonstrate a useful technique to investigate the shielding applications of MGF materials.

4.1 Magnetic Field Shielding Effectiveness

We measured the magnetic field SE by using the near-field technique (see sect. 2.1) for various MGF samples, where the resin type, vacuum conditions, and sample thicknesses (i.e., the number of layers) are the param-

eters that are varied. Figure 13 shows the near-field SE data for one layer of MGF pressed under vacuum and also cured using epoxy resin (using the best vacuum possible). Note the low-frequency noise from the power service and the spurious data near 10 MHz for the uncured MGF not under vacuum. These data are repeatable and represent E-field coupling to the receive antenna cables. This spurious coupling is normally negligible, but can be seen for samples that exhibit very little SE, and can be removed by using optical isolation on the receive antenna. The epoxy-cured sample for this test started with the first piece of MGF mat taken from the roll, which appeared to have a lower MGF density than subsequent samples.

Figure 14 shows the SE result for two layers of MGF mat held under vacuum or cured using epoxy resin. The rest of the cured samples are more typical of MGF mat than the initial one-layer sample. Note the repeatability of the bare MGF mat (i.e., 0 in. Hg) for two layers compared to the data for one layer (see fig. 13). The epoxy-cured sample did not obtain as high an SE as the bare MGF mat under vacuum, due to the high viscosity of this resin. The data then indicated that a lower viscosity resin was required for uniform wetting of the MGF, so polyester resin was used

Figure 13. Near-field test results for one layer of MGF mat.
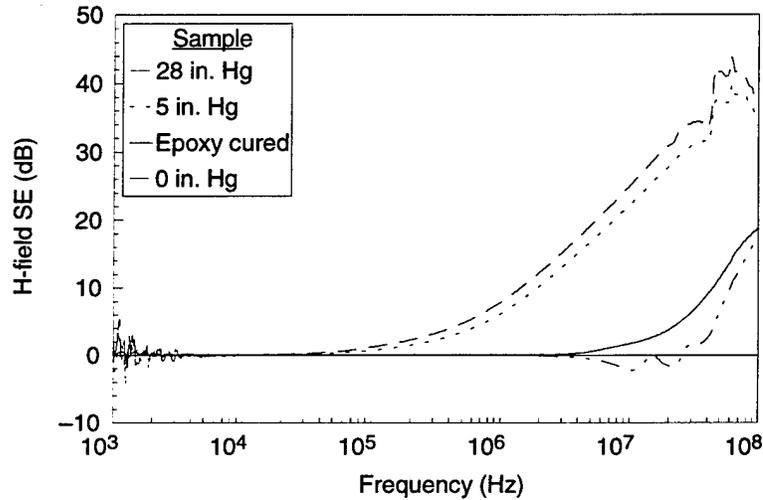
Figure 14. Near-field test results for two layers of MGF mat.

20
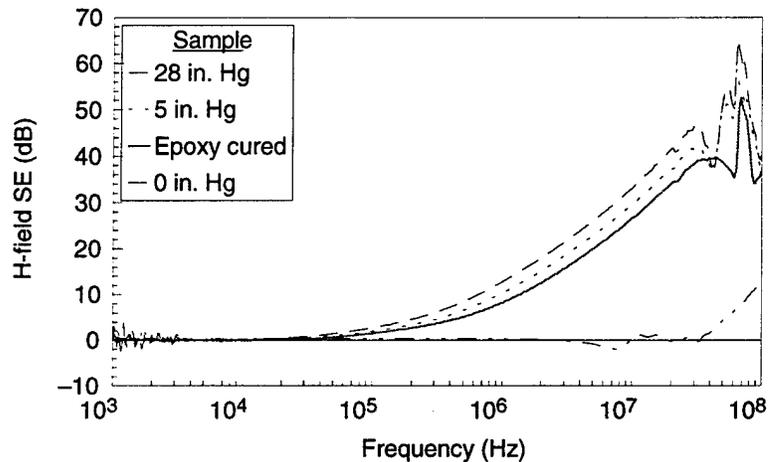
for the rest of the cured MGF samples. Figure 15 summarizes the near-field SE data for one layer of MGF mat, where it can be seen that the polyester-resin-cured sample exhibits the best SE. Uniform wetting of the MGF mat provides for closer contact between the conductive members and, hence, a better SE. The measured H-field SE for the MGF enclosure is also shown for comparison. Figure 16 summarizes the near-field and enclosure SE data for two layers of MGF mat. The measured SE for the enclosure is much less than could be obtained with polyester-resin-cured samples under vacuum, since the best vacuum obtainable for the enclosure was only about 5 in. Hg.

4.2   Plane Wave Shielding Effectiveness

Attenuation measurements were performed at the SMF on both a cured MGF mat and an uncured MGF mat. A measurement sensitivity improvement was brought about by including a 23-dB preamplifier before the oscilloscope. This amplification aids in overcoming the sampling head noise floor, but does not help with the data lost through cable attenuation. The preamplifier was used when measuring the fields with and without the MGF mat in place. This ensures that the amplifier characteristics cancel when the SE is calculated. Precision attenuators with flat response in the frequency range required were used when measuring the direct field.

Figure 15. Near-field test summary for one layer of MGF mat.
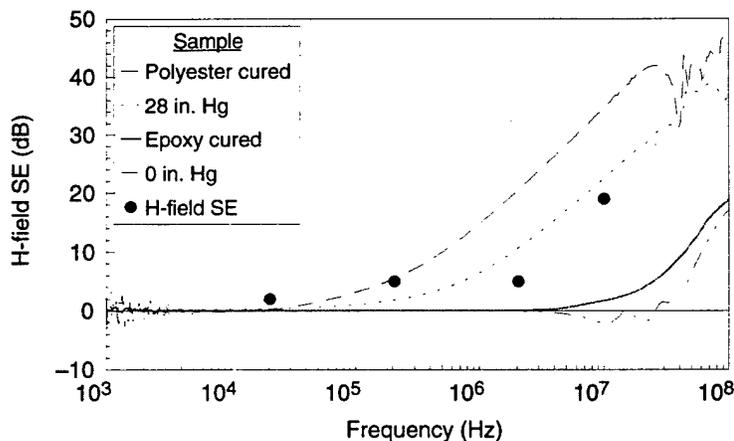
Figure 16. Near-field test summary for two layers of MGF mat.
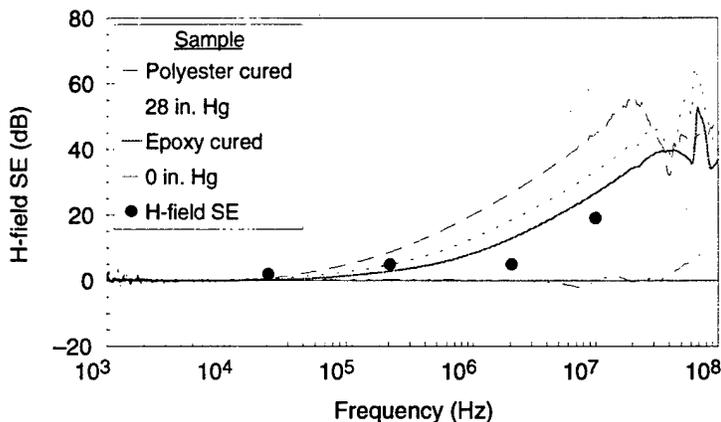
The incident and attenuated E-dot data for the cured MGF panel are shown in figure 17. Based on the circuit model for shielding [16], a material time constant can be identified as

$$\tau \equiv \mu\sigma t^2 . \tag{8}$$

For the single-layer panel with overlapped seams of vacuum-cured MGF, the thickness is nonuniform and ranges from $\frac{1}{32}$ to $\frac{1}{16}$ in. Thus the average thickness is $t = 1.2$ mm, and a typical $\sigma_{eff} = 1$ kS/m can be determined from the near-field test data. Under these assumptions, the EM diffusion time, $T_c \approx \tau/4$, is 600 ps, which is in excellent agreement with the measured 600-ps time delay shown in figure 17.

The measured SE as a function of frequency is determined by Fourier inversion of the measured incident and attenuated transients. This frequency-domain ratio is interpreted as the shielding versus frequency and is consistent with other continuous wave (cw) measurement techniques. The results for the uncured and cured panels are shown in figures 18(a) and (b), respectively. The theoretical results (see sect. 3) for a $\frac{1}{16}$-in. panel are shown for comparison with σ_{eff} as a parameter. As can be seen, the wideband pulse attenuation results are completely consistent with plane-wave shielding theory, subject to the assumptions employed for the material parameters. The measured data are consistent with the typical conductivity (1 kS/m) found in the laboratory tests.

4.3   Enclosure Shielding Effectiveness

The shielded enclosure was tested according to IEEE-STD-299-1991, with some modifications, at frequencies up to 19 GHz. The test data demonstrated that the seam treatments were fairly effective, but the leakage around the metal door limited the enclosure SE at high frequencies. The results are presented as recommended by the test standard in each of the frequency ranges. The results for each TP are based on the largest received signal in the scanning procedure for that TP.

Figure 17. Incident and attenuated E-dot data for cured MGF mat.

22
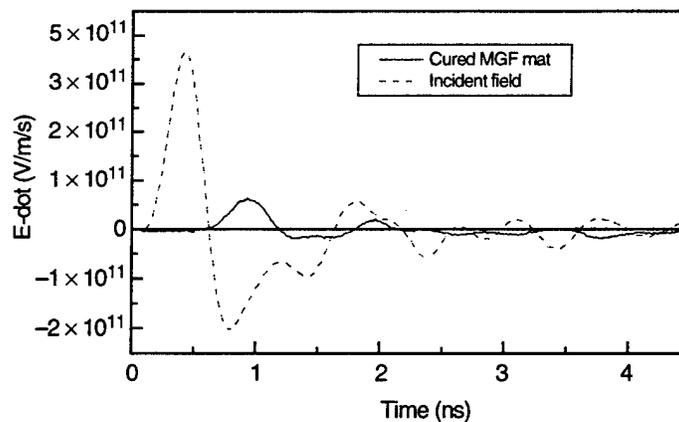
Figure 18. Pulse attenuation versus frequency: (a) uncured MGF mat and (b) uncured and polyester resin-cured MGF mat.

(a)

Legend:
— Measured
⋯ 100 mho/m
– – 10 mho/m
–·– Absorption

(b)

Legend:
— Uncured
– – – Cured
–□– σ_{eff} = 1 kS/m
–○– σ_{eff} = 2 kS/m
–△– σ_{eff} = 5 kS/m
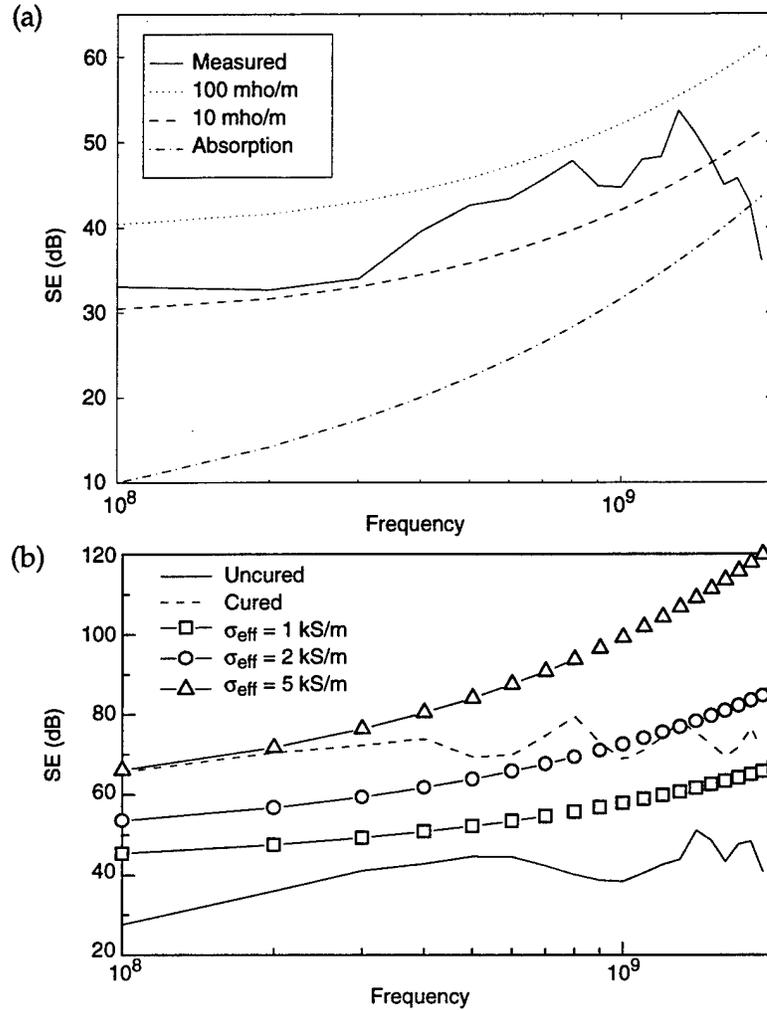
4.3.1 Low-Range Measurements

The substitution technique quantifies the measured SE, and the average of all measurements was calculated according to IEEE-STD-299-1991. This average is included even for the H-field SE measurements, as shown in table 5.

4.3.2 Mid-Range Measurements

For comparison to the mid-frequency plane wave SE data, the TDFD result for the E-field inside the composite enclosure is converted to the frequency domain. The enclosure SE is calculated in the frequency domain as the ratio of the E-field 9 in. inside the enclosure and the incident E-field at this location in the absence of the shelter. The comparison is shown in figure 19 with the limited amount of averaged plane wave SE data in this frequency range. Also shown is the TDFD result for the estimated thickness of MGF (σ_{eff} = 1 kS/m) required to obtain 80 dB of shielding.

23

Table 5. MGF enclosure SE test results at low- and mid-range frequencies.

Test point	Polarization	H-field Antenna separation: 24.5 in.				Plane wave 72 in.		
		20 kHz	200 kHz	2 MHz	10 MHz	300 MHz	600 MHz	900 MHz
D1	V	2	4	5	7	56	44	33
D2	H	3	5	6	20	59	57	44
D3	H	3	6	5	24	64	64	45
D4	V	2	4	3	18	51	54	55
D5	H	3	5	5	20	54	59	56
D6	H	3	4	6	18	52	56	55
D7	H	7	9	9	26	62	67	53
D7	V	4	6	5	21	51	48	41
S1	H	0	1	0	14	51	67	48
S1	V	0	1	0	9	60	54	51
S2	H	0	5	7	23	54	70	53
S2	V	0	3	5	20	63	69	44
S3	H	1	1	0	15	68	70	53
S3	V	2	3	0	10	56	56	53
V2	H	2	5	6	17	59	66	51
V2	V	2	4	4	21	58	71	52
C2	H	2	7	7	20	62	58	52
C2	V	3	6	5	14	65	48	43
Average level (dB)		2	5	5	19	60	63	51

Figure 19. TDFD enclosure SE result at 9 in. behind front face for $\sigma = 1$ kS/m.
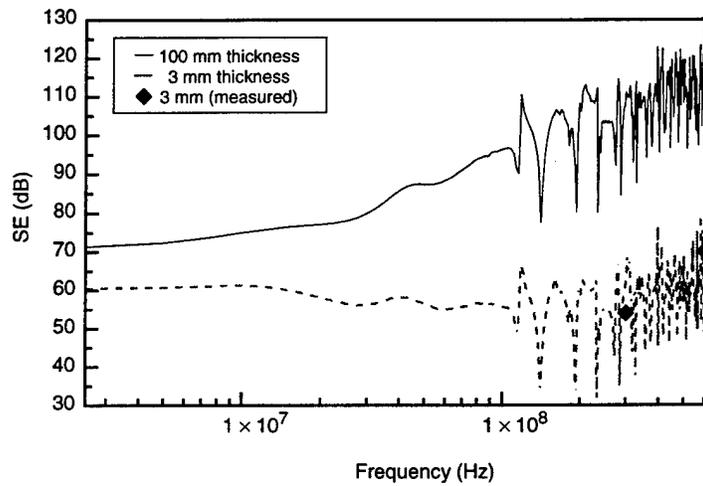
4.3.3 High-Range Measurements

Table 6 summarizes the high-range test results. As the tests progressed, several test points were dropped because of the misleading results they produced. All test points in close proximity to the door show contributions from seam leakage around the door, resulting in low shielding values. The door used had a very poor RF seal (light could be seen through the seams), which contributes to the lower shielding data for all measurements near or on the rear plane. The door does not represent a

24

Table 6. High-range SE test results for MGF enclosure.

Test point	Frequency (GHz)	Minimum SE (dB) and receive antenna orientation	
		Vertical source antenna	Horizontal source antenna
D7	1	45.0 V	58.0 H
S1	1	59.5 V	60.0 H
V1	1	52.5 H	57.3 45°
V2	1	50.8 V	62.0 H
C1	9	50.0 V	53.2 V
C2	9	51.5 V	53.0 45°
D1	9	45.0 V	56.0 H
D7	9	—	59.0 H
D8	9	55.0 V	48.8 H
S1	9	76.0 V	77.8 H
S2	9	80.7 45°	77.8 H
S3	9	73.2 45°	73.2 45°
T1	9	55.0 V	57.2 45°
T2	9	59.0 V	65.3 V
V1	9	71.7 V	51.5 H
V2	9	77.2 V	74.8 45°
V3	9	77.0 45°	77.2 H
V4	9	68.3 45°	60.3 45°
C1	17	56.3 V	55.5 H
C2	17	66.5 V	70.5 45°
D7	17	63.3 V	62.5 H
D8	17	64.2 V	51.5 H
S1	17	>79	>79
S3	17	>79	>79
T1	17	59.5 V	63.5 45°
T2	17	65.3 V	72.0 H
V1	17	71.5 H	47.3 H
V3	17	>79	>79
V4	17	69.7 45°	55.8 H

commercial production and should not be considered in determining the gross performance of the mock-up shelter. The objective of the test was to evaluate the SE of cured MGF mat, and the formation of seams with this material, for shelter-size enclosures.

In general, at the higher frequencies, local features and flaws are detectable through shielding measurements. For example, shielding is worse near the door than on the sides or front, which indicates local sources in this area that are associated with seam leakage around the door. At 1 GHz, local features are not as pronounced, yet rear test points are still higher than test points on the front and side.

4.3.4 Standardized Test Results

The SE test data demonstrated that the enclosure seam treatments were fairly effective, but the leakage around the door limited the measured SE at high frequencies. As recommended by the test standard, the results are averaged and presented in each of the frequency ranges. The substitution technique quantifies the measured SE, and the results are summarized in table 7. The dip in SE at 900 MHz could be due to the receive antenna

Table 7. Standardized SE test results (in dB) for MGF enclosure.

Frequency	Type of measurement	Local source		Distant source	
		With door	Without door	With door	Without door
20 kHz	H-field	0	0	2	0
200 kHz	H-field	1	1	5	4
2 MHz	H-field	0	0	5	4
10 MHz	H-field	7	9	19	17
300 MHz	Plane wave	51	51	60	61
600 MHz	Plane wave	44	48	63	66
900 MHz	Plane wave	33	43	51	51
1 GHz	Plane wave	45	51	56	57
9 GHz	Plane wave	45	50	64	66
17 GHz	Plane wave	52 (47)	56 (47)	67	68

size, which is near resonance at this frequency. The door used had a poor RF seal, so the standardized results (given in table 7) are presented both with and without the door SE data included in the average value. A hole developed in the floor near the door, which also affected the SE data for nearby locations at 17 GHz.

5. Conclusion

MGF materials are of interest as an integral shielding approach to control electromagnetic interference/electromagnetic compatibility (EMI/EMC) in advanced military systems or subsystems. The EM properties of chopped MGF composite panels have been well documented; however, incorporating MGF mat directly into composite layups may be more practical. For this reason, we investigated the shielding performance of MGF nonwoven mat as obtained from the manufacturer versus the composite curing process parameters. Since enclosure SE depends on the shielded volume-to-surface ratio, we also constructed a full-scale model of an Army tactical shelter suitable for standardized SE testing. This experiment demonstrated that the design and construction practices would be critical issues in producing a reliable and maintainable composite system capable of meeting military SE requirements.

The laboratory test results indicated that the MGF conductivity (hence, the SE) is highly dependent on the composite curing process, especially when used in the mat form. The experimental results confirmed that uniform resin wetting and close contact of the metallized fiber is critical for obtaining an optimum conductivity in the finished sample. Thus, a low-viscosity resin and high-vacuum curing would be recommended to maximize the effective conductivity of MGF composites. Although the MGF mat may be an efficient way of incorporating conductive particles into composite parts, the volume fraction of fibers can be more difficult to control, because the fiber density in the nonwoven mat is not uniform. Thus, multiple-layer layups or chopped strand mold processes would be

recommended for optimizing the effective conductivity of MGF composites.

We chose a two-layer dry layup and vacuum curing to construct a full-scale MGF model of an Army tactical shelter. The enclosure SE was measured according to standardized test methods, and the plane-wave SE data were consistent with the wideband pulse attenuation experimental results. The enclosure provided about 60 dB plane wave SE, but almost no magnetic field shielding. Thus, for extremely broadband shielding applications, the metallized particle density would have to increase substantially or magnetic materials would be required. The latter is recommended, by the addition of either a magnetic MGF or metallized particles (e.g., nickel-coated microspheres) to the composite material. The analytical and numerical results demonstrate that simplifying assumptions (e.g., an effective conductivity that is uniform and isotropic) can be used at radio frequencies. In particular, EMA3D provides plane-wave SE results for composite enclosures that are consistent with the standardized test data.

The construction and subsequent SE testing of the full-scale shelter model confirmed the lessons learned in the laboratory, namely, that medium-level SE can be readily obtained using metallized particles, but that incorporating MGF into a shielded system introduces design and engineering issues that must be solved cost-effectively. Since good conductivity and electrical continuity are required throughout the shielded enclosure, panel or modular construction techniques would require good electrical joining and bonding to avoid seam leakage at high frequencies. Since the SE of MGF improves at high frequency, a shielded design to meet medium-level SE requirements should be straightforward. However, research in the performance and use of conductive adhesives with MGF and the appropriate surface preparation would be required. Thus MGF would be best used in near-net-shape manufacturing processes that would allow the incorporation of MGF (magnetic and/or nonmagnetic) in a uniform manner. The treatment of penetrations and grounding practices then become engineering issues, which can be solved using shielded enclosure design practices that allow for the reduced conductivity of MGF compared to metallic systems. The investigations summarized here provide baseline data and analytical approaches for developing a shielded composite system by integrating MGF materials during the composite construction. However, the use of these advanced materials must be incorporated throughout the system design, development, production, and deployment in order to meet broadband SE requirements over the system life cycle.

6. References

1. R. H. Warfel, *Optimum Performance of Metallized Glass Fiber-Filled Composites*, 35th Annual Technical Conference, Society of Plastics Industry, Sec. 19-E (1980), pp 1–6.

2. D. M. Bigg, *Mechanical, Thermal, and Electrical Properties of Metal Fiber-Filled Polymer Composites*, Society of Plastic Engineers, Inc., 37th Annual Technical Conference (1979), p 583.

3. R. J. Chase, *Composite Shielding Initiative for Army Resources*, U.S. Army Research Laboratory, ARL-SR-9 (June 1994).

4. J. Latess, C. D. Le, and J. V. Jaucian, *Investigations on the Use of Near Field Measurements to Determine the Effective Conductivity of Advanced Composite Materials*, U.S. Army Research Laboratory, ARL-TR-707 (July 1995).

5. R. C. Johnson, *Antenna Engineering Handbook*, 3rd edition, McGraw-Hill Book Company, Inc., New York (1993).

6. D. F. Straw and L. D. Piszker, *Interaction of Advanced Composites with Electromagnetic Environment*, Boeing Aerospace Company, AFML-TR-75-141 (September 1975).

7. L. V. King, *Electromagnetic Shielding at Radio Frequencies*, Phil. Mag. J. Sci. **15** (February 1993), pp 201–223.

8. A. A. Cuneo, Jr., and J. J. Loftus, *Measurement of Scaled-Down HEMP Waveforms*, Harry Diamond Laboratories, HDL-TM-81-6 (March 1981).

9. J. J. Loftus, V. Fronczak, and I. Kohlberg, *A Comparison of the Diffracted Fields as Measured and Predicted for a Totally Reflecting Fence in a Scale Model Test for an EMP Simulator*, Harry Diamond Laboratories, HDL-TR-2173 (February 1990).

10. W. O. Coburn and C. G. Reiff, *Wideband Pulse Attenuation of an Uncured Metallized Glass Fiber Mat*, U.S. Army Research Laboratory, ARL-TR-790 (September 1995).

11. S. A. Schelkunoff, *Electromagnetic Waves*, Van Nostrand, Princeton, NJ (1943).

12. R. B. Schultz et al, *Shielding Theory and Practice*, Trans EMC **30** (August 1988), pp 187–201.

13. D. White, *A Handbook on Electromagnetic Shielding Materials and Performance*, Don White Consultants, Inc. (1975).

14. EMA3D User Manual, Electro Magnetic Applications, Inc., EMA-95-R-012 (February 1995).

15. P. M. McKenna, T. H. Rudolph, and R. A. Perala, *A Time Domain Representation of Surface and Transfer Impedance Useful for Analysis of Advanced Composite Aircraft*, Proceedings of the International Aerospace and Ground Conference on Lightning and Static Electricity (June 1984).

16. R. L. Monroe, *Research in Electromagnetic Shielding Theory: Part I. Shielding by Rectangular Enclosures*, Harry Diamond Laboratories, HDL-CR-88-052-1 (March 1988).

Distribution

Admnstr
Defns Techl Info Ctr
Attn DTIC-OCP
8725 John J. Kingman Rd Ste 0944
FT Belvoir VA 22060-6218

Dir
Defns Intllgnc Agcy
Attn RTS-2A Techl Lib
Washington DC 20301

Defns Special Weapons Agcy
Attn RAES Elect Syst Techlgy Div
Attn RAST Electromagnetic Applctn Div
Attn TITL Tech Lib
6801 Telegraph Rd
Alexandria VA 22310-3398

Defns Special Weapons Agcy
Office of Techl Applications
Attn D R Lewis
Alexandria VA 22310

Cmdr
US Army ARDEC
Attn AMSTA-AR-AEC-IE N Svendsen
Picatinny Arsenal NJ 07806-5000

US Army AVRDEC
Attn AMSAT-R-EFM P Haselbauer
4300 Goodfellow Blvd
ST Louis MO 63120-1798

US Army BRDEC
Attn SATB-FGE J Ferrick
Attn SATB-FGE T Childers
FT Belvoir VA 22060-5606

US Army Matl Cmnd
Attn AMCAM-CN
5001 Eisenhower Ave
Alexandria VA 22333-0001

Dir
US Army Mis Cmnd (USAMICOM)
Attn AMSMI-RD-CS-R Documents
Redstone Arsenal AL 35898-5400

Cmdr
US Army MRDEC
Attn AMSMI-RD-ST-CM J Vandier
Huntsville AL 35898-5240

US Army Natick RDEC
Attn SATNC-SUSD-SHD A Murphy
Kansas Stret
Natick MA 01760-5018

US Army Nuc & Chem Agcy
Attn MONA-NU R Pfeffer
7150 Heller Loop Rd Ste 101
Springfield VA 22150

US Army Rsrch Lab
Attn AMSRL-SL-CS B Smith
Aberdeen Proving Gound MD 21010-5423

Cmdr
US Army TARDEC
Attn AMSTA-ZT G Baker
Warren MI 48397-5000

US Army TECOM
Attn STERT-TE-E J Knaur
Redstone Technical Test Center
Huntsville AL 35898-8052

US Army TECOM Techl Dir Ofc
Attn AMSTE-TC-D R Bell
Aberdeen Proving Ground MD 21005

Cmdr
US Army White Sands Missile Range
Attn STEWS-NE J Meason
White Sands Missile Range NM 88002-5180

Nav Rsrch Lab
Attn Code 4820 Techl Info Div
4555 Overlook Ave SW
Washington DC 20375-5000

Cmdr
Nav Surfc Weapons Ctr
Attn Code E231 Techl Lib
Dahlgren VA 22448-5020

Distribution

Natl Inst of Stand & Techlgy
Attn V Ulbrecht Rsrch Info Ctr
Rm E01 Bldg 101
Gaithersburg MD 20899

Hdqrts Dept of the Army
Attn DAMO-FDT D Schmidt
400 Army Pentagon Rm 3C514
Washington DC 20310-0460

US Military Academy
Dept of Mathematical Sci
Attn MDN-A Maj D Engen
West Point NY 10996

Palisades Inst for Rsrch Svc Inc
Attn E Carr
1745 Jefferson David Hwy Ste 500
Arlington VA 22202-3402

Ofc of the Dir Rsrch and Engrg
Attn R Menz
Pentagon Rm 3E1089
Washington DC 20301-3080

Ofc of the Secy of Defns
Attn ODDRE (R&AT) G Singley
Attn ODDRE (R&AT) S Gontarek
The Pentagon
Washington DC 20301-3080

OSD
Attn OUSD(A&T)/ODDDR&E(r) R Tru
Washington DC 20301-7100

CECOM
Attn PM GPS COL S Young
FT Monmouth NJ 07703]

CECOM RDEC Elect System Div Dir
Attn J Niemela
FT Monmouth NJ 07703

CECOM
Sp & Terrestrial Commctn Div
Attn AMSEL-RD-ST-MC-M H Soicher
FT Monmouth NJ 07703-5203

Dir of Assessment and Eval
Attn SARD-ZD H K Fallin Jr
103 Army Pentagon Rm 2E673
Washington DC 20310-0163

MICOM RDEC
Attn AMSMI-RD W C McCorkle
Redstone Arsenal AL 35898-5240

US Army Avn Rsrch, Dev, & Engrg Ctr
Attn T L House
4300 Goodfellow Blve
St Louis MO 6321-1798

US Army CECOM Rsrch, Dev, & Engrg
Attn R F Giordano
FT Monmouth NJ 07703-5201

US Army Edgewood Rsrch, Dev, & Engrg Ctr
Attn SCBRD-TD J Vervier
Aberdeen Proving Ground MD 21010-5423

US Army Info Sys Engrg Cmd
Attn ASQB-OTD F Jenia
FT Huachuca AZ 85613-5300

US Army Materiel Sys Analysis Agcy
Attn AMXSY-D J McCarthy
Aberdeen Proving Ground MD 21005-5071

US Army Matl Cmnd
Dpty CG for RDE Hdqtrs
Attn AMCRD BG Beauchamp
5001 Eisenhower Ave
Alexandria VA 22333-0001

US Army Matl Cmnd
Prin Dpty for Acquisition Hdqrts
Attn AMCDCG-A D Adams
5001 Eisenhower Ave
Alexander VA 22333-0001

US Army Matl Cmnd
Prin Dpty for Techlgy Hdqrts
Attn AMCDCG-T M Fisette
5001 Eisenhower Ave
Alexandria VA 22333-0001

US Army Natick Rsrch, Dev, & Engrg Ctr
Acting Techl Dir
Attn SSCNC-T P Brandler
Natick MA 01760-5002

Distribution

US Army Rsrch Ofc
Attn G Iafrate
4300 S. Miami Blvd
Research Triangle Park NC 27709

US Army Simulation, Train, & Instrmntn Cmd
Attn J Stahl
12350 Research Parkway
Orlando FL 32826-3726

US Army Tank-Automtv & Armaments Cmd
Attn AMSTA-AR-TD C Spinelli
Bldg 1
Picatinny Arsenal NJ 07806-5000

US Army Tank-Automtv Cmd Rsrch, Dev, &
   Engrg Ctr
Attn AMSTA-TA J Chapin
Warren MI 48397-5000

US Army Test & Eval Cmd
Attn R G Pollard III
Aberdeen Proving Ground MD 21005-5055

US Army Train & Doctrin Cmd
Battle Lab Integration& Techl Dirctrt
Attn ATCD-B J A Klevecz
FT Monroe VA 23651-5850

USAASA
Attn MOAS-AI W Parron
9325 Gunston Rd Ste N319
FT Belvoir VA 22060-5582

Nav Surface Warfare Ctr
Attn Code B07 J Pennella
17320 Dahlgren Rd Bldg 1470 Rm 1101
Dahlgren VA 22448-5100

GPS Joint Prog Ofc Dir
Attn COL J Clay
2435 Vela Way Ste 1613
Los Angeles AFB CA 90245-5500

DARPA
Attn B Kaspar
Attn L Stotts
3701 N Fairfax Dr
Arlington VA 22203-1714

ARL Electromag Group
Attn Campus Mail Code F0250 A Tucker
University of Texas
Austin TX 78712

Dir for MANPRINT
Ofc of the Dpty Chief of Staff for Prsnnl
Attn J Hiller
The Pentagon Rm 2C733
Washington DC 20310-0300

 US ARDEC
Attn AMSTA-AR-AEF-A Chf
Adelphi MD 20783-11987

US Army Rsrch Lab
Attn AMSRL-CS-AL-TA Mail & Records
   Mgmt
Attn AMSRL-CI-LL Tech Library (3 copies)
Attn AMSRL-CS-AL-TP Tech Pub (3 copies)
Attn AMSRL-SE Chf
Attn AMSRL-SE-D Chf
Attn AMSRL-SE-DS Chf
Attn AMSRL-SE W O Coburn (10 copies)
Attn AMSRL-SE-DP Chf
Attn AMSRL-SE-D Sr Rsrch Scntst
Attn AMSRL-WT-PB Chf
Attn AMSRL-WT-WB Chf
Attn AMSRL-WT-WC Chf
Attn AMSRL-WT-WD Chf
Adelphi MD 20783-1197

REPORT DOCUMENTATION PAGE

Form Approved
OMB No. 0704-0188

1. AGENCY USE ONLY *(Leave blank)*	2. REPORT DATE March 1998	3. REPORT TYPE AND DATES COVERED Final, FY96

4. TITLE AND SUBTITLE

Investigations on the Broadband Shielding Effectiveness of Metallized Glass Fiber

5. FUNDING NUMBERS

PE: 62120A

6. AUTHOR(S)

William O. Coburn, John Latess, Christian G. Reiff, Vincent J. Ellis, James Stewart, and Calvin D. Le

7. PERFORMING ORGANIZATION NAME(S) AND ADDRESS(ES)

U.S. Army Research Laboratory
Attn: AMSRL-SE-DS (wcoburn@arl.mil)
2800 Powder Mill Road
Adelphi, MD 20783-1197

8. PERFORMING ORGANIZATION REPORT NUMBER

ARL-TR-1376

9. SPONSORING/MONITORING AGENCY NAME(S) AND ADDRESS(ES)

U.S. Army Research Laboratory
2800 Powder Mill Road
Adelphi, MD 20783-1197

10. SPONSORING/MONITORING AGENCY REPORT NUMBER

11. SUPPLEMENTARY NOTES

AMS code: 622120.H25
ARL PR: 6WN534

12a. DISTRIBUTION/AVAILABILITY STATEMENT

Approved for public release; distribution unlimited.

12b. DISTRIBUTION CODE

13. ABSTRACT *(Maximum 200 words)*

Metallized glass fiber (MGF) is a glass fiber substrate with a metal coating that can be used to improve the electrical properties of reinforced composites. The material considered here (RoMHOglas™-metallized glass conductive fibers produced by Lundy Technical Center, Pompano Beach, Florida) is an E-glass fiber metallized with Al and processed into a nonwoven mat. When formed into a mat, the MGFs lead to an effective sample conductivity, σ_{eff}, which is the parameter of interest for electromagnetic shielding in the RF region. Experimental results are presented that show that σ_{eff} is dependent on the resin and curing process used to produce the MGF samples. The sample conductivity was optimized using polyester resin and vacuum bagging techniques. The lessons learned were used to construct an MGF-shielded Army tactical shelter-size enclosure having no apertures or penetrations other than the door opening.

(continued on back)

14. SUBJECT TERMS

Shielding effectiveness, metallized glass fiber, RoMHOglas™, enclosure shielding

15. NUMBER OF PAGES
42

16. PRICE CODE

17. SECURITY CLASSIFICATION OF REPORT Unclassified	18. SECURITY CLASSIFICATION OF THIS PAGE Unclassified	19. SECURITY CLASSIFICATION OF ABSTRACT Unclassified	20. LIMITATION OF ABSTRACT UL

13. Abstract (cont'd)

   We applied two layers of the MGF mat to the interior surfaces of a plywood, full-scale model of an Army tactical shelter. Using overlapping seams, we secured the MGF layers to the plywood walls and sprayed them with polyester resin. A vacuum bag was fitted to the interior and exterior of the shelter model. A vacuum was applied to compress the two layers of MGF mat and remove excess resin. A metal door with an eight-cleat clamping arrangement and an electromagnetic interference gasket was used to provide a continuously shielded enclosure. This shielded enclosure was then tested according to IEEE-STD-299-1991, with some modifications, at frequencies up to 17 GHz. The results are presented as recommended by the test standard and indicate that compressed MGF mat can provide roughly 60 dB of attenuation to a distant source, but very little shielding below 10 MHz.